Available online at www.sciencedirect.com

ScienceDirect

Advances in Space Research 67 (2021) 3396–3408

ADVANCES IN SPACE RESEARCH (a COSPAR publication)

www.elsevier.com/locate/asr

Spacecraft formation and orbit control using differential attitude-dependent solar radiation pressure

Ethan R. Burnett *, Hanspeter Schaub

Ann and H.J. Smead Department of Aerospace Engineering Sciences, University of Colorado Boulder, 3775 Discovery Dr, Boulder, CO 80303, USA

Received 4 November 2019; received in revised form 4 February 2020; accepted 29 March 2020
Available online 12 April 2020

Abstract

This paper introduces a linear model for spacecraft formation dynamics subject to attitude-dependent solar radiation pressure (SRP) disturbance, with the SRP model accounting for both absorption and specular/diffuse reflection. Spacecraft attitude is represented in modified Rodriguez parameters (MRPs), which also parameterize the orientation of individual facets for a spacecraft with fixed geometry. Compared to earlier work, this model incorporates analytic approximation of the SRP-perturbed chief orbit behavior in a manner enabling its use in applications with infrequent guidance updates. Control examples are shown for single-plate representations of hypothetical spacecraft with generally realistic optical parameters. The results demonstrate the validity of the model and the feasibility of SRP-based formation and rendezvous control in orbits around small bodies and in high orbits around the Earth such as the GEO belt.

Keywords: Formation flying; Solar radiation pressure; Linear controls; Perturbations; Dynamics

1. Introduction

Solar radiation pressure (SRP) is the driving force for solar sails, but it is typically viewed as a disturbance force and not a control parameter for typical modern spacecraft. However, in environments where differential solar radiation pressure is sufficiently strong on the scale of the relative motion dynamics, small sustained variations in attitude can be used to harness this perturbation for control – even for spacecraft without sails. While not particularly suitable in low-Earth orbits, the efficacy of this control method becomes much greater for multi-spacecraft formations sufficiently far from the planet. The geostationary (GEO) region is one example. In this region, the spacecraft are not subject to strong disturbances from higher-order gravitational effects or drag due to the rarefied atmosphere. For example, at GEO, the SRP disturbance on a BSS-702 Bus is nearly as influential as the third-body disturbance, and on the same order as the effect of the of accelerations from the low-order zonal harmonics (Vallado, 2007). The differential acceleration between two nearby spacecraft at this altitude has the potential to be much larger for SRP than for the other disturbances, because it scales with differences in illuminated spacecraft area while the other differential accelerations scale with separation. SRP-based control also becomes a feasible option for formations in orbit around small bodies such as asteroids, comets, and moons.

SRP-based control is conceptually similar to differential drag-based control strategies that already fly, except this perturbation is typically not fixed in a particular direction in the LVLH frame (Foster et al., 2018). Furthermore, unlike with differential drag, the direction of the resultant disturbance acceleration vector can be partially articulated by rotating the spacecraft about the axis aligned with the direction to the sun. The possibility of using small attitude changes for formation-keeping is appealing because of the

* Corresponding author.
E-mail address: ethan.burnett@colorado.edu (E.R. Burnett).

https://doi.org/10.1016/j.asr.2020.03.047
0273-1177/

potential for saved thruster fuel. It is also valuable because the differential SRP force between identical spacecraft can achieve the incredibly small values necessary for real-time and high-precision formation-keeping around small asteroids and comets. Even the smallest commercially available ion thrusters could be too powerful to generate the small forces needed for continuous control in station-keeping or high precision formation control in these environments, requiring them to be used in a pulsed control strategy almost like chemical thrusters. This contradicts the nature of their design for very long-duration burns, reducing efficiency and accelerating wear. Other design solutions are available to partially mitigate this issue, such as pulsed plasma thrusters (PPTs), but these are not as efficient as other forms of electric propulsion. In this context, SRP-based control might be preferred over any type of electric propulsion, and can be implemented on spacecraft with traditional geometry and surface materials.

The topic of natural SRP-perturbed orbital dynamics has been frequently studied, especially in the vicinity of small bodies (Scheeres, 2012). Many works use a cannonball SRP model, and focus on finding stable orbits while assuming the force variation with attitude is not significant (Dankowicz, 1994; Byram and Scheeres, 2009). Some works also discuss orbit-attitude coupling in the uncontrolled dynamics, or the coupled effects of multiple perturbations (Kikuchi et al., 2017; Misra et al., 2016; Lantukh et al., 2015). Recent work by Kenshiro Oguri and Jay McMahon focuses on SRP-based orbit control around asteroids (Oguri and McMahon, 2018). The optical force SRP model used in their work is essentially equivalent to the one used here, but their approach is otherwise quite different. Their work studies orbit control via a chosen subset of the orbit elements, namely semimajor axis and inclination. The optimal attitude for control is parameterized by two angles, whose values are obtained numerically based on the current system state. The paper makes multiple novel analytical arguments that provide insight about the controlled orbital dynamics – including attitude constraints to prevent orbital escape, and even an analytic upper bound for the time of flight for landing on an asteroid using SRP-based control.

It is worth noting that SRP-based control has also been extensively studied for solar sails (McInnes, 1999; Dachwald, 2010; Parsay and Schaub, 2015; Parsay and Schaub, 2016). Because sails are designed to make the maximum use of solar radiation pressure, these works typically make restrictive assumptions about the spacecraft geometry or optical properties. While interesting work has been done to study the natural and controlled orbital dynamics using the SRP force, this paper is focused on the topic of orbital formation control, for which spacecraft with traditional geometry and design can still produce sufficient differences in SRP force to use it as a relative position and velocity control parameter.

In contrast to the previously mentioned works on the topic of SRP-based control, a desirable approach would be to use a relative motion model that requires only occasional updates of the spacecraft orbital elements of one or more of the spacecraft in the formation. Ideally, a model accounting for the evolution of the perturbed orbit and the linearized SRP-perturbed differential dynamics will naturally enable sufficiently reliable situational awareness even with low navigation update frequency. Lastly, linearization leverages the smallness of the formation geometry on the scale of the spacecraft orbits, by allowing for a suitable linear control law to be developed. Namely, it is amenable to a linearly optimal LQR control approach – in which the optimal gain schedule can be computed in advance of the maneuver, or in a receding-horizon manner. Developing such a model is the primary focus of this paper.

This paper derives a linearized time-varying (LTV) model of formation dynamics subject to attitude-dependent SRP forces. The problem geometry for a single illuminated spacecraft facet is given in Fig. 1 for a spacecraft that seeks to rendezvous with a nearby chief spacecraft using only the attitude-controlled SRP forces $\sum_i \boldsymbol{F}_{S_i}$ for control. The relative state is resolved in local radial, transverse, and normal directions, which use the chief position vector $\boldsymbol{r}$ and angular momentum vector $\boldsymbol{h}$ as $\hat{\boldsymbol{e}}_r = \boldsymbol{r}/r, \hat{\boldsymbol{e}}_t = -\hat{\boldsymbol{e}}_r \times \hat{\boldsymbol{e}}_h$, and $\hat{\boldsymbol{e}}_h = \boldsymbol{h}/h$. The vector $\hat{\boldsymbol{u}}$ points towards the sun and $\hat{\boldsymbol{H}}$ is normal to the planet orbit plane. The model uses the deputy-chief notation commonly used in spacecraft formation flying, in which the motion of one spacecraft (the deputy) is described with respect to another (the chief), in a local chief-centered frame. The model may be updated with chief orbit elements with any desired frequency. Analytical approaches such as the one used in this paper naturally allow for the evolution of the spacecraft orbit elements to be approximated for relatively long timespans, i.e. for several orbits in the numerical examples. This model can easily be combined with components of other models to account for additional system perturbations, such as the low-order gravitational harmonics (Burnett and Butcher, 2018). While it is assumed that updated relative heading, range, and range-rate data is periodically available for the spacecraft in the formation, the relative position and velocity can be efficiently integrated between measurements using the linearized model. By incorporating accurate and computationally efficient approximation of system evolution into the model, significant decoupling of the tasks of control and navigation is achievable. Overall, the developments in this paper are a step towards enabling a highly flexible, simple formation control strategy suitable for closed-loop SRP-based spacecraft formation control.

This work introduces and develops SRP-based control for the relative motion of multiple 3-axis stabilized spacecraft in similar orbits, with similar geometry and optical properties. Assumptions inherent to the approach are that the deputy-chief separation is small on the scale of the chief orbit, and that the deputy attitude deviations from the reference orientation are well-represented by a linearization in

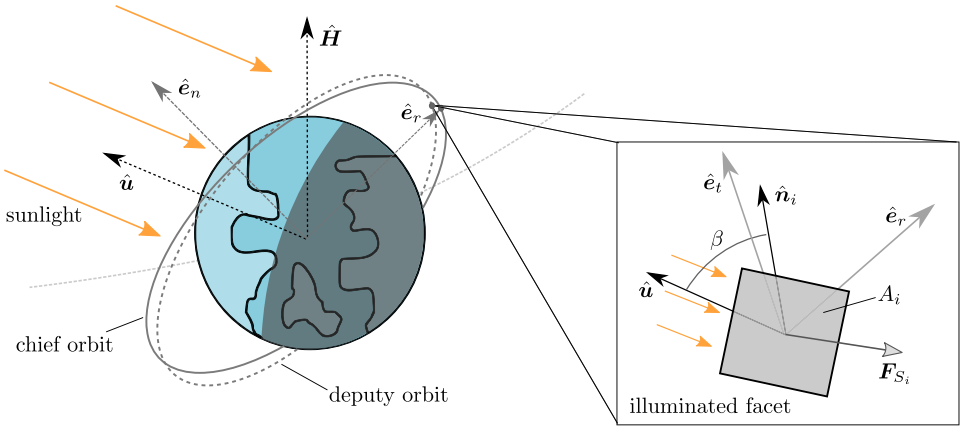

Fig. 1. Problem Geometry for SRP-based Control, with Attitude-Dependent Resultant Force $\boldsymbol{F}_{S_i}$.

modified Rodriguez parameters (MRPs). In this control formulation, the chief and deputy are thus assumed to have similar attitudes. Small variations in the deputy attitude from the chief attitude induce differences in the resultant SRP acceleration between the spacecraft. The formulation is introduced in a way that can be extended to enable control with a time-varying chief reference attitude, but for simplicity the chief attitude is assumed to be fixed with respect to the sun. For the proof-of-concept simulations, the model is implemented with a single facet only, but the approach can be easily generalized to a multi-facet spacecraft model. The approach developed in this paper could be adapted and extended to find use in future multi-spacecraft missions to asteroids and comets, and will also be useful for formation control or orbit maintenance in high-altitude orbits about the Earth, such as the GEO belt.

Lastly, it is important to note that the use of SRP for spacecraft control has already been demonstrated in flight. The K2 mission was able to make use of SRP effects to extend the life of the Kepler space telescope mission, which was suffering from attitude control under-actuation due to reaction wheel failure. This was done by achieving and maintaining an orientation to passively minimize the SRP disturbance along the roll axis (Howell et al., 2014). The Messenger mission to Mercury used SRP for precision orbit control, which is particularly notable and relevant to this work. In that mission, pre-planned attitude and solar array articulations were used to improve the accuracy of Mercury flybys (O'Shaughnessy et al., 2009). This was done in an open-loop fashion, but closed-loop control would be highly desirable. Closed-loop control should be readily achievable using SRP models with varying levels of fidelity, and the work in this paper enables further steps towards that goal.

2. Spacecraft formation dynamics with solar radiation pressure

The force due to solar radiation pressure on a general body surface element A_i is given below (Scheeres, 2007):

$$\boldsymbol{F}_{S_i} = -P(R)H_i(\hat{\boldsymbol{u}})A_i\Big[\Big(\rho_i s_i\Big(2\hat{\boldsymbol{n}}_i\hat{\boldsymbol{n}}_i - \overline{\overline{\boldsymbol{I}}}\Big) + \overline{\overline{\boldsymbol{I}}}\Big)\cdot\hat{\boldsymbol{u}}(\hat{\boldsymbol{u}}\cdot\hat{\boldsymbol{n}}_i) + a_{2i}\hat{\boldsymbol{n}}_i(\hat{\boldsymbol{n}}_i\cdot\hat{\boldsymbol{u}})\Big] \tag{1}$$

with

$$P(R) \approx \frac{G_1}{R^2} \tag{2}$$

$$a_{2i} = B(1-s_i)\rho_i + (1-\rho_i)B \tag{3}$$

The function $P(R)$ is the solar radiation pressure at distance R, and G_1 is the solar radiation force constant at 1 AU. The term $\overline{\overline{\boldsymbol{I}}}$ is the identity dyad, for which $\overline{\overline{\boldsymbol{I}}}\cdot\boldsymbol{r} = \boldsymbol{r}$ for any vector $\boldsymbol{r}$. Likewise, $\hat{\boldsymbol{n}}_i\hat{\boldsymbol{n}}_i$ is a dyad for which $\hat{\boldsymbol{n}}_i\hat{\boldsymbol{n}}_i\cdot\boldsymbol{r} = (\hat{\boldsymbol{n}}_i\cdot\boldsymbol{r})\hat{\boldsymbol{n}}_i$ (Danielson, 2003). The specular and diffuse reflectivity coefficients are s_i and ρ_i, and B is the Lambertian scattering coefficient, $\hat{\boldsymbol{u}}$ is the unit vector to the sun, $\hat{\boldsymbol{n}}_i$ is the normal vector of the surface element, and $H_i(\hat{\boldsymbol{u}})$ is a visibility delta function, equal to 1 or 0, depending on whether or not the face is directly illuminated by sunlight. Fig. 1 highlights the important aspects of the problem geometry.

For simplicity and generality, this analysis neglects the effects of secondary reflections from other surfaces. However, a realistic treatment of the body optical properties (B, s_i, ρ_i) is important.

The SRP force can be modeled by considering the sum of the forces on all illuminated facets. The results in this paper use a single-facet model of a spacecraft for generality and to validate the derivation. However, it is emphasized that this method can be directly generalized to a spacecraft with fixed geometry and multiple illuminated facets. Summing over the contributions of all body area elements, an approximate model of the net SRP force vector on the spacecraft is obtained:

$$\boldsymbol{F}_S = -P(R)A\big(\big(\overline{a}_2\cos\beta + 2\overline{\rho s}\cos^2\beta\big)\hat{\boldsymbol{n}} + (1-\overline{\rho s})\cos\beta\hat{\boldsymbol{u}}\big) \tag{4}$$

where $\cos\beta = \hat{\boldsymbol{u}}\cdot\hat{\boldsymbol{n}}$, A is a projected area term, and $\hat{\boldsymbol{n}}$ is the corresponding equivalent normal unit vector. This implementation neglects the eclipse dynamics, but the effect

could easily be re-introduced for a higher fidelity control implementation. The terms $\overline{a}_2, \overline{\rho}$, and $\overline{s}$ are illuminated body-averaged optical parameters. This replaces the multi-facet SRP force model with a single-plate SRP force model at some reference orientation. It is always possible to obtain an equivalent single-plate model representation of the resultant SRP force acting on a spacecraft, for which the sum of the $\hat{\boldsymbol{n}}_i$ components of the resultant SRP force acts along $\hat{\boldsymbol{n}}$, and the $\hat{\boldsymbol{u}}$ component is also reproduced. However, the extent to which attitude-dependent SRP force variations of the single plate correctly model the true spacecraft SRP force variations is situation dependent. Accuracy would be highly dependent on spacecraft geometry and the optical properties of the surface facets.

Other approaches of modeling SRP acceleration variation for small angles are possible, such as a local linearization of the spherical harmonic series representation (Farrés et al., 2017). The purpose of this work is to demonstrate the feasibility of using attitude-dependent SRP acceleration for formation and rendezvous control, so studies of the control implications of SRP model fidelity are left for future work.

2.1. Problem geometry and coordinate frames

Before continuing with the derivation of the linearized dynamics and control model, the primary coordinate frames must be defined. First, the rotating frame moving with the primary body is called the planet frame $\mathcal{P}$, and is defined by orthonormal vectors $\left\{\hat{\boldsymbol{u}}, \hat{\boldsymbol{H}} \times \hat{\boldsymbol{u}}/\|\hat{\boldsymbol{H}} \times \hat{\boldsymbol{u}}\|, \hat{\boldsymbol{H}}\right\}$, where $\hat{\boldsymbol{u}}$ points from the planet toward the sun and $\hat{\boldsymbol{H}} = \boldsymbol{h}_p/h_p$ is defined by the planet's orbit angular momentum vector $\boldsymbol{h}_p$, normal to its orbit plane.

Fig. 2 shows the relationship between the $\mathcal{N}$ and $\mathcal{P}$ frames. One can describe the rotation from the planet frame to the primary-centered inertial ($\mathcal{N}$) frame through two angles:

$$[\mathcal{NP}] = [R_1(\kappa)][R_3(\varphi+\pi)]^\top = \begin{bmatrix} -\cos\varphi & \sin\varphi & 0 \\ -\sin\varphi\cos\kappa & -\cos\varphi\cos\kappa & \sin\kappa \\ \sin\varphi\sin\kappa & \cos\varphi\sin\kappa & \cos\kappa \end{bmatrix} \tag{5}$$

where $[R_1(\theta)]$ denotes the rotation matrix for a 1-axis rotation by angle θ, and $[R_3(\theta)]$ is the rotation matrix for a 3-axis rotation by angle θ (Schaub and Junkins, 2018). The angle κ is the obliquity of the ecliptic plane and φ is the argument of latitude, or the rotation angle (in the orbit plane) from the Vernal Equinox to the radial vector from the sun to the planet. For Earth, $\kappa \approx 23.5°$, and the $\mathcal{N}$ frame is the typical Earth-centered inertial (ECI) frame.

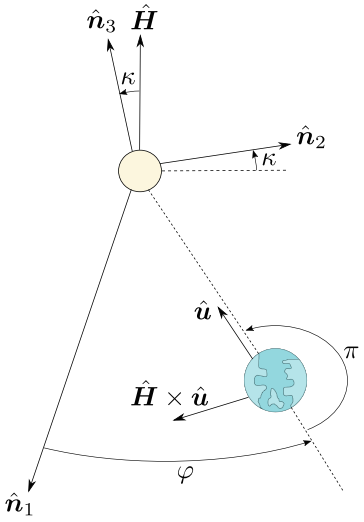

Fig. 2. Coordinate Frames $\mathcal{N}$ and $\mathcal{P}$.

Because this paper is focused on using SRP force for rendezvous and formation control, the controlled relative motion of two or more spacecraft is considered. The spacecraft labeling deputy and chief is commonly used in formation flying literature. The motions of one or more deputies relative to the chief are used to describe formation or rendezvous geometry without explicitly considering all individual spacecraft orbits. Note that one may arbitrarily decide which spacecraft is designated as the chief and which is the deputy. In this paper, the chosen representation for the relative state is to resolve the relative position

$$\Delta\boldsymbol{r} = [x, y, z]^\top \tag{6}$$

and velocity

$$\Delta\boldsymbol{r}' = [\dot{x}, \dot{y}, \dot{z}]^\top \tag{7}$$

in the chief-centered rotating local-vertical, local-horizontal (LVLH) frame. Here, $()'$ denotes the derivative of a state quantity as seen in the LVLH frame. This frame rotates with the spacecraft orbit and is defined by orthonormal radial, along-track, and orbit-normal vectors $\{\hat{\boldsymbol{e}}_r, \hat{\boldsymbol{e}}_t, \hat{\boldsymbol{e}}_n\}$. The radial and normal unit vectors are defined in the usual way, in terms of the chief spacecraft position $\boldsymbol{r}$ and velocity $\boldsymbol{v}$: $\hat{\boldsymbol{e}}_r = \boldsymbol{r}/r$ and $\hat{\boldsymbol{e}}_n = \boldsymbol{r} \times \boldsymbol{v}/\|\boldsymbol{r} \times \boldsymbol{v}\|$.

A final rotation from the inertial frame to an orbiting spacecraft-centered local-vertical local-horizontal (LVLH frame) may now be defined. The rotation $[\mathcal{HN}]$ is given below in terms of the chief spacecraft orbit radial and angular momentum vectors $\boldsymbol{r}$ and $\boldsymbol{h}$, and equivalently in a 3–1–3 sequence in terms of the spacecraft orbit elements Ω, i, and $\theta = \omega + f$ (Schaub and Junkins, 2018):

$$[\mathcal{HN}] = \begin{bmatrix} \cos\Omega\cos\theta - \sin\Omega\sin\theta\cos i & \sin\Omega\cos\theta + \cos\Omega\sin\theta\cos i & \sin\theta\sin i \\ -\cos\Omega\sin\theta - \sin\Omega\cos\theta\cos i & -\sin\Omega\sin\theta + \cos\Omega\cos\theta\cos i & \cos\theta\sin i \\ \sin\Omega\sin i & -\cos\Omega\sin i & \cos i \end{bmatrix} \tag{9}$$

$$[\mathcal{HN}] = \begin{bmatrix} \hat{\boldsymbol{r}}^\top \\ \frac{1}{r\hbar}(r^2\boldsymbol{v} - (\boldsymbol{v}\cdot\boldsymbol{r})\boldsymbol{r})^\top \\ \hat{\boldsymbol{h}}^\top \end{bmatrix} \tag{8}$$

Thus, the rotation from $\mathcal{P}$ to $\mathcal{H}$ is:

$$[\mathcal{HP}] = [\mathcal{HN}][\mathcal{NP}] \tag{10}$$

With the system geometry and coordinate descriptions now defined, a control matrix $[B]$ can be obtained, which maps deputy spacecraft attitude deviations to accelerations in the LVLH frame. The uncontrolled dynamics of an SRP-perturbed multi-spacecraft formation are also considered to obtain the system matrix $[A]$. The derivation of the linearized system matrix $[A]$ of the relative dynamics is more involved than the derivation of $[B]$, and therefore is carried out is a subsequent part of the work.

2.2. Linearized attitude-based SRP control

Modified Rodrigues Parameters (MRPs) are used to describe the spacecraft attitude, or the attitude of a single-plate model in this paper. This attitude description is expressed in terms of the principal rotation elements (angle α and axis $\hat{\boldsymbol{e}}$) (Schaub and Junkins, 2018):

$$\boldsymbol{\sigma} = \tan\frac{\alpha}{4}\hat{\boldsymbol{e}} \tag{11}$$

The MRP attitude representation has the benefit of linearizing as $\boldsymbol{\sigma} \approx (\alpha/4)\hat{\boldsymbol{e}}$, providing a larger usable range for linear control than an angular representation (Schaub and Junkins, 2018).

The mapping to and from a general rotation matrix $[C]$ is given below:

$$[C] = [I_{3\times3}] + \frac{8[\tilde{\boldsymbol{\sigma}}]^2 - 4(1-\sigma^2)[\tilde{\boldsymbol{\sigma}}]}{(1+\sigma^2)^2} \tag{12}$$

$$\boldsymbol{\sigma} = \begin{pmatrix} \sigma_1 \\ \sigma_2 \\ \sigma_3 \end{pmatrix} = \frac{1}{\zeta(\zeta+2)} \begin{pmatrix} C_{23} - C_{32} \\ C_{31} - C_{13} \\ C_{12} - C_{21} \end{pmatrix} \tag{13}$$

where $\zeta = \sqrt{C_{11} + C_{22} + C_{33} - 1}$, $\sigma^{2n} = (\boldsymbol{\sigma}^\top\boldsymbol{\sigma})^n$, and $[\tilde{\boldsymbol{\sigma}}]$ is the MRP skew-symmetric matrix.

To use the MRP formulation, the rotation of a vector in $\mathcal{P}$ components into the spacecraft body frame ($\mathcal{B}$) components is defined in terms of two successive rotations. The first is a rotation $[C_1(\boldsymbol{\sigma}_r)]$ to the "reference" attitude, and the second is a rotation $[C_2(\boldsymbol{\sigma}_c)]$ to the current orientation, which is a controlled deviation from this reference attitude:

$${}^{\mathcal{B}}\boldsymbol{r} = [C_2(\boldsymbol{\sigma}_c)][C_1(\boldsymbol{\sigma}_r)]{}^{\mathcal{P}}\boldsymbol{r} \tag{14}$$

The attitude deviation $\boldsymbol{\sigma}_c$ is the control parameter for attitude-based position control using SRP. This work assumes that the spacecraft attitude control system is fully capable of enforcing the needed attitude behavior.

From Eq. 4, substituting $\hat{\boldsymbol{n}}\cdot\hat{\boldsymbol{u}}$ for all $\cos\beta$ terms, the force due to SRP is rewritten below in its $\mathcal{P}$ components using ${}^{\mathcal{P}}\hat{\boldsymbol{n}} = [C_1(\boldsymbol{\sigma}_r)]^\top[C_2(\boldsymbol{\sigma}_c)]^\top{}^{\mathcal{B}}\hat{\boldsymbol{n}}$ and defining ${}^{\mathcal{B}}\hat{\boldsymbol{n}} = \hat{\boldsymbol{e}}_1$ and ${}^{\mathcal{P}}\hat{\boldsymbol{u}} = \hat{\boldsymbol{e}}_1$, where $\hat{\boldsymbol{e}}_1 = [1,0,0]^\top$:

$$\begin{aligned}\boldsymbol{F}_S = -P(R)A\Big(&\Big(\overline{a}_2(\hat{\boldsymbol{n}}\cdot\hat{\boldsymbol{u}}) + 2\overline{\rho s}(\hat{\boldsymbol{n}}\cdot\hat{\boldsymbol{u}})^2\Big)[C_1(\boldsymbol{\sigma}_r)]^\top[C_2(\boldsymbol{\sigma}_c)]^\top \\ &+(1-\overline{\rho s})(\hat{\boldsymbol{n}}\cdot\hat{\boldsymbol{u}})[I_{3\times3}])\hat{\boldsymbol{e}}_1\end{aligned} \tag{15}$$

To obtain the $[B]$ matrix, this equation must be linearized with respect to the control term $\boldsymbol{u} = \boldsymbol{\sigma}_c$. First, all control-associated parts are replaced with their expansions up to $O(\sigma_c)$:

$$[C_2(\boldsymbol{\sigma}_c)] \approx [I_{3\times3}] - 4[\tilde{\boldsymbol{\sigma}}_c] \tag{16}$$

$$\begin{aligned}\hat{\boldsymbol{n}}\cdot\hat{\boldsymbol{u}} &= \hat{\boldsymbol{e}}_1^\top[C_2(\boldsymbol{\sigma}_c)][C_1(\boldsymbol{\sigma}_r)]\hat{\boldsymbol{e}}_1 \\ &\approx \hat{\boldsymbol{e}}_1^\top([C_1(\boldsymbol{\sigma}_r)] - 4[\tilde{\boldsymbol{\sigma}}_c][C_1(\boldsymbol{\sigma}_r)]\hat{\boldsymbol{e}}_1)\end{aligned} \tag{17}$$

$$(\hat{\boldsymbol{n}}\cdot\hat{\boldsymbol{u}})^2 \approx \big(\hat{\boldsymbol{e}}_1^\top[C_1(\boldsymbol{\sigma}_r)]^\top\hat{\boldsymbol{e}}_1\big)\hat{\boldsymbol{e}}_1^\top([C_1(\boldsymbol{\sigma}_r)] - 8[\tilde{\boldsymbol{\sigma}}_c][C_1(\boldsymbol{\sigma}_r)]\hat{\boldsymbol{e}}_1) \tag{18}$$

Substituting Eqs. (16)–(18) into Eq. (15), expanding, and retaining only terms up to $O(\sigma_c)$, the linearization of $\boldsymbol{F}_S$ is obtained:

$$\begin{aligned}\boldsymbol{F}_S \approx\ & -P(R)A\big\{\big(\overline{a}_2 + 2\overline{\rho s}\hat{\boldsymbol{e}}_1^\top[C_1(\boldsymbol{\sigma}_r)]\hat{\boldsymbol{e}}_1\big)\big) \\ &\times\big(\hat{\boldsymbol{e}}_1^\top[C_1(\boldsymbol{\sigma}_r)]\hat{\boldsymbol{e}}_1\big([C_1(\boldsymbol{\sigma}_r)]^\top([I_{3\times3}] + 4[\tilde{\boldsymbol{\sigma}}_c])\big)\big) \\ &-4\big(\overline{a}_2 + 4\overline{\rho s}\hat{\boldsymbol{e}}_1^\top[C_1(\boldsymbol{\sigma}_r)]\hat{\boldsymbol{e}}_1\big)\hat{\boldsymbol{e}}_1^\top[\tilde{\boldsymbol{\sigma}}_c][C_1(\boldsymbol{\sigma}_r)]\hat{\boldsymbol{e}}_1[C_1(\boldsymbol{\sigma}_r)]^\top \\ &+(1-\overline{\rho s})\hat{\boldsymbol{e}}_1^\top([I_{3\times3}] - 4[\tilde{\boldsymbol{\sigma}}_c])\hat{\boldsymbol{e}}_1[I_{3\times3}]\big\}\hat{\boldsymbol{e}}_1\end{aligned} \tag{19}$$

This equation is linear in $\boldsymbol{\sigma}_c$, and is rearranged below so that the control vector $\boldsymbol{\sigma}_c$ is explicitly isolated:

$$\begin{aligned}\boldsymbol{F}_S = \ & -P(R)A\big\{\big(\overline{a}_2 + 2\overline{\rho s}C_{1(1,1)}\big)\big(C_{1(1,1)}[C_1(\boldsymbol{\sigma}_r)]^\top\big)\hat{\boldsymbol{e}}_1 \\ &-4\big(\overline{a}_2 + 2\overline{\rho s}C_{1(1,1)}\big)\big(C_{1(1,1)}[C_1(\boldsymbol{\sigma}_r)]^\top[\tilde{\boldsymbol{e}}_1]\big)\boldsymbol{\sigma}_c \\ &-4\big(\overline{a}_2 + 4\overline{\rho s}C_{1(1,1)}\big)\big([C_1(\boldsymbol{\sigma}_r)]^\top\big[\hat{\boldsymbol{e}}_1\hat{\boldsymbol{e}}_1^\top\big][C_1(\boldsymbol{\sigma}_r)]^\top[\tilde{\boldsymbol{e}}_1]\big)\boldsymbol{\sigma}_c \\ &+(1-\overline{\rho s})\hat{\boldsymbol{e}}_1 + 4(1-\overline{\rho s})\big[\hat{\boldsymbol{e}}_1\hat{\boldsymbol{e}}_1^\top\big][\tilde{\boldsymbol{e}}_1]\boldsymbol{\sigma}_c\big\}\end{aligned} \tag{20}$$

where the shorthand notation $C_{1(1,1)} = \hat{\boldsymbol{e}}_1^\top[C_1(\boldsymbol{\sigma}_r)]\hat{\boldsymbol{e}}_1$ is used. Note that the terms premultiplying $\boldsymbol{\sigma}_c$ Eq. (20) represents the general control matrix $[B]$ for the system resolved in $\mathcal{P}$. For a time-varying reference orientation, this matrix is time-varying.

For the proof-of-concept simulations in this work, it is assumed that the reference orientation is sun-facing, then

$[C_1(\boldsymbol{\sigma}_r)] = [I_{3\times3}]$ and a simpler form is obtained for the single facet model:

$$\boldsymbol{F}_S = -P(R)A\{(1+\overline{\rho s}+\overline{a}_2)\hat{\boldsymbol{e}}_1 - 4(\overline{a}_2+2\overline{\rho s})[\tilde{\boldsymbol{e}}_1]\boldsymbol{\sigma}_c\} \tag{21}$$

From this result, the $[B]$ matrix can be isolated for the system resolved in $\mathcal{P}$:

$$[B] = 4\frac{P(R)A}{m}\begin{bmatrix} & \boldsymbol{0}_{4\times3} & \\ 0 & 0 & -\overline{a}_2-2\overline{\rho s} \\ 0 & \overline{a}_2+2\overline{\rho s} & 0 \end{bmatrix} \tag{22}$$

Again, note that the $[B]$ matrix for a more general reference orientation can be readily obtained by isolating the control-associated terms in Eq. (20). This can also be easily resolved in any desired frame by using the appropriate rotation matrices. Note that in the case of linearization about a sun-facing reference, the $[B]$ matrix for the system resolved in $\mathcal{P}$ predicts zero acceleration will be produced along the $\hat{\boldsymbol{u}}$ direction due to small controlled attitude variations. In reality, a small acceleration will be produced, but this is not captured by the linearization. This suggests that for a sun-facing reference, motion along the $\hat{\boldsymbol{u}}$ direction is instantaneously uncontrollable with linear control. However, investigations later in the paper show that the system is still fully controllable.

2.3. Linearized relative motion dynamics under SRP

Having a system matrix $[A]$ that incorporates the perturbative effects of SRP on the relative motion dynamics will enable better control performance than by using a system matrix that doesn't account for the perturbation, such as the popular Hill-Clohessy-Wiltshire (HCW) model (Clohessy and Wiltshire, 1960). This section provides a derivation of a model for uncontrolled SRP-perturbed relative orbital motion behavior of the spacecraft, suitable for use with the proof-of-concept control implementations.

Because the SRP-based control is enabled by deviations from a reference attitude that is assumed to be fixed in the $\mathcal{P}$ frame, this analysis assumes that if the two spacecraft are at the same orientation, then the SRP-based differential acceleration between the deputy and chief spacecraft is negligible. This implicitly assumes that the deputy and chief geometry and optical characteristics are similar. In this case, with both spacecraft at the same orientation with respect to the sun, the only manifestation of the SRP acceleration is on the kinematics of the chief-centered LVLH frame. Note that depending on the dynamic environment, this effect may be overshadowed by other disturbance accelerations.

The angular velocity of the perturbed LVLH frame with respect to the inertial frame may be described in terms of the perturbed orbit element rates (Casotto, 2016):

$$\boldsymbol{\omega}_H = \frac{d\Omega}{\mathrm{d}t}\hat{\boldsymbol{a}}_3 + \frac{\mathrm{d}i}{\mathrm{d}t}\frac{\hat{\boldsymbol{a}}_3\times\hat{\boldsymbol{e}}_n}{\|\hat{\boldsymbol{a}}_3\times\hat{\boldsymbol{e}}_n\|} + \frac{\mathrm{d}\theta}{\mathrm{d}t}\hat{\boldsymbol{e}}_n \tag{23}$$

where $\hat{\boldsymbol{a}}_3$ is the vector pointing along the planet polar axis, the third orthogonal unit vector used for the $\mathcal{N}$ frame. The angle Ω is the right ascension of the ascending node, i is the inclination, and $\theta = \omega + f$ is the argument of latitude. The orbit element rates are obtained using the variational equations in their Gaussian form to yield the osculating rates due to the SRP perturbation, resolved in local radial, along-track, and cross-track components:

$$\boldsymbol{a}_{\mathrm{SRP}} = R_{\mathrm{SRP}}\hat{\boldsymbol{e}}_r + T_{\mathrm{SRP}}\hat{\boldsymbol{e}}_t + N_{\mathrm{SRP}}\hat{\boldsymbol{e}}_n \tag{24}$$

$$\frac{d\Omega}{dt} = \frac{r\sin\theta}{h\sin i}N_{\mathrm{SRP}} \tag{25a}$$

$$\frac{\mathrm{d}i}{\mathrm{d}t} = \frac{rcos\theta}{h}N_{\mathrm{SRP}} \tag{25b}$$

$$\frac{\mathrm{d}\theta}{\mathrm{d}t} = \frac{\mathrm{d}\omega}{\mathrm{d}t} + \frac{\mathrm{d}f}{\mathrm{d}t} = \frac{h}{r^2} - \frac{r\sin\theta\cos i}{h\sin i}N_{\mathrm{SRP}} \tag{25c}$$

The argument of latitude is used to avoid the possibility of small denominators in the variational equations for near-circular orbits. The argument of latitude rate has two components: the "unperturbed" argument of latitude rate $\dot{\theta}_u = h/r^2$, and a component due to the regression of the node from which θ is measured (Prussing and Conway, 2013). The expression for N_{SRP} may be obtained using the rotation from $\mathcal{P}$ to $\mathcal{H}$, and the SRP disturbance force resolved in $\mathcal{P}$ components, Eq. (20), with $\boldsymbol{\sigma}_c = \boldsymbol{0}$ because the chief attitude is the reference orientation. In this analysis, it is assumed that the chief attitude is fixed in the $\mathcal{P}$ frame.

$$N_{\mathrm{SRP}} = \frac{1}{m}\hat{\boldsymbol{e}}_3^{\top}[\mathcal{HN}][\mathcal{NP}]\boldsymbol{F}_S \tag{26}$$

$$N_{\mathrm{SRP}} = -P(R)\frac{A}{m}\left(\frac{(1-\overline{\rho s})}{C_{1(1,1)}} + \overline{a}_2 + 2\overline{\rho s}C_{1(1,1)}\right) C_{1(1,1)}\left(\hat{\boldsymbol{e}}_3^{\top}[HN][NP][C_1(\boldsymbol{\sigma}_r)]^{\top}\hat{\boldsymbol{e}}_1\right) \tag{27}$$

$$N_{\mathrm{SRP}} = -P(R)\frac{A}{m}\left(\frac{(1-\overline{\rho s})}{C_{1(1,1)}} + \overline{a}_2 + 2\overline{\rho s}C_{1(1,1)}\right) C_{1(1,1)}\left(\hat{\boldsymbol{e}}_{\xi}^{\top}[C_1(\boldsymbol{\sigma}_r)]^{\top}\hat{\boldsymbol{e}}_1\right) \tag{28}$$

where the unit vector $\hat{\boldsymbol{e}}_{\xi}$ is not a function of θ due to the problem geometry:

$$\hat{\boldsymbol{e}}_{\xi} = \begin{pmatrix} \sin\kappa\sin\varphi\cos i - \sin\Omega\cos\varphi\sin i + \cos\Omega\cos\kappa\sin\varphi\sin i \\ \sin\kappa\cos\varphi\cos i + \sin\Omega\sin\varphi\sin i + \cos\Omega\cos\kappa\cos\varphi\sin i \\ \cos\kappa\cos i - \cos\Omega\sin\kappa\sin i \end{pmatrix} \tag{29}$$

Assuming the primary body orbit radius R is nearly constant and that the reference orientation is stationary as seen in the $\mathcal{P}$ frame, the only time-varying term in Eq. (28) is the primary body's argument of latitude, φ. Generally, this time scale will be much slower than the spacecraft orbit period about the primary body, and may be slow enough to ignore for sufficiently short-duration rendezvous.

By applying the transport theorem twice with angular velocity given by Eq. (23), the kinematics of the perturbed LVLH frame are given in radial, along-track, and cross-track components:

$$\begin{aligned}\Delta\ddot{\boldsymbol{r}} = \quad & \left(\ddot{x} - \dot{\omega}_n y - 2\omega_n \dot{y} - \omega_n^2 x + \omega_n \omega_r z\right)\hat{\boldsymbol{e}}_r \\ & + \left(\ddot{y} + \dot{\omega}_n x + 2\omega_n \dot{x} - \left(\omega_n^2 + \omega_r^2\right) y - \dot{\omega}_r z - 2\omega_r \dot{z}\right)\hat{\boldsymbol{e}}_t \\ & + \left(\ddot{z} + \omega_n \omega_r x + \dot{\omega}_r y + 2\omega_r \dot{y} - \omega_r^2 z\right)\hat{\boldsymbol{e}}_n\end{aligned} \tag{30}$$

where the angular velocity has also been resolved into its LVLH components:

$$\omega_r = \dot{\Omega}\frac{\sin i}{\sin\theta} \tag{31a}$$

$$\omega_t = 0 \tag{31b}$$

$$\omega_n = \dot{\theta}_u = h/r^2 \tag{31c}$$

The term $\Delta\ddot{\boldsymbol{r}}$ represents the differential perturbing accelerations. If only the SRP differential acceleration is considered, then, in the case of the earlier listed assumptions, this term is due only to the differential gravity, which is assumed to be a two-body potential for now:

$$\Delta\ddot{\boldsymbol{r}}_{J_0} = \frac{\mu}{r^3}\begin{pmatrix} 2x \\ -y \\ -z \end{pmatrix} \tag{32}$$

The choice of local Cartesian/curvilinear coordinates for treatment of the perturbed relative motion problem has led to one important limitation: large chief orbit eccentricities introduce significant analytical difficulties to the derivation, for multiple reasons. While such problems are still analytically tractable, this derivation is restricted to cases of $e \approx 0$ (near-circular orbits) and $\dot{a} \approx 0$ (negligible changes to orbit specific energy). This dynamical model can theoretically be adapted for perturbed eccentric orbits, assuming $\dot{e} \approx 0$ still holds, and that all ρ terms are updated to account for the variations in the chief radius. Note that writing $\dot{e} \approx 0$ only implies the assumption that the effects from $\dot{e}$ are small compared to the first-order effects of the solar radiation pressure. However, this will not always be the case. Both the long and short-term effects of solar radiation pressure on eccentricity are discussed extensively by Scheeres (2012). Relaxing of the aforementioned assumptions and further potential developments of the model are left to future work.

To first order in the SRP terms, assuming $\dot{a} \approx 0$ and $\dot{e} \approx 0$, it can be shown that the only nonzero angular acceleration term is $\dot{\omega}_r$, given below with the nonzero angular velocity squared terms:

$$\dot{\omega}_r = n\frac{\sin i}{\sin\theta}\left(\frac{\mathrm{d}}{\mathrm{d}\theta}\left(\dot{\Omega}\right) - \dot{\Omega}\frac{\cos\theta}{\sin\theta}\right) + \dot{\varphi}\frac{\sin i}{\sin\theta}\frac{\mathrm{d}}{\mathrm{d}\varphi}\left(\dot{\Omega}\right) \tag{33}$$

$$\omega_n\omega_r = n\rho_r^{-3/2}\dot{\Omega}\frac{\sin i}{\sin\theta} \tag{34}$$

$$\omega_n^2 = \frac{h^2}{r^4} \tag{35}$$

where $\rho_r = r/a$ and n is the orbital mean motion. From the near-circular orbit assumption and the assumption $\dot{a} \approx 0$, it is implied that $r(t) \approx a$, thus $\dot{\theta}_p \approx n$ and $\rho_r \approx 1$. These assumptions will not be valid for long time spans if the SRP disturbance acceleration is large enough to significantly change the chief orbit. Evaluating Eqs. 35,33,34, all nonzero kinematic terms are presented below, explicitly in terms of N_{SRP}:

$$\omega_r = \frac{r}{h}N_{\mathrm{SRP}},\ \ \omega_n = \frac{h}{r^2} \tag{36}$$

$$\dot{\omega}_r = \dot{\varphi}\frac{r}{h}\frac{\mathrm{d}}{\mathrm{d}\varphi}(N_{\mathrm{SRP}}) \tag{37}$$

$$\omega_n\omega_r = n\rho_r^{-3/2}\frac{r}{h}N_{\mathrm{SRP}},\ \ \omega_n^2 = \frac{h^2}{r^4} \tag{38}$$

The final linearized relative motion equations are obtained and presented below in matrix-vector form, resolved in the chief-centered LVLH frame, $\mathcal{H}$.

$$\begin{aligned}\begin{pmatrix}\ddot{x}\\ \ddot{y}\\ \ddot{z}\end{pmatrix} = & \begin{bmatrix} h^2/r^4 + 2\frac{\mu}{r^3} & 0 & -n\rho^{-3/2}\frac{r}{h}N_{\mathrm{SRP}} \\ 0 & h^2/r^4 - \frac{\mu}{r^3} & \dot{\varphi}\frac{r}{h}\frac{\mathrm{d}}{\mathrm{d}\varphi}(N_{\mathrm{SRP}}) \\ -n\rho^{-3/2}\frac{r}{h}N_{\mathrm{SRP}} & -\dot{\varphi}\frac{r}{h}\frac{\mathrm{d}}{\mathrm{d}\varphi}(N_{\mathrm{SRP}}) & -\frac{\mu}{r^3}\end{bmatrix}\begin{pmatrix}x\\ y\\ z\end{pmatrix} \\ & + \begin{bmatrix} 0 & 2\frac{h}{r^2} & 0 \\ -2\frac{h}{r^2} & 0 & 2\frac{r}{h}N_{\mathrm{SRP}} \\ 0 & -2\frac{r}{h}N_{\mathrm{SRP}} & 0\end{bmatrix}\begin{pmatrix}\dot{x}\\ \dot{y}\\ \dot{z}\end{pmatrix}\end{aligned} \tag{39}$$

If small variations in the chief orbit radius are known, and any resulting terms are of the same order as linear SRP-associated terms, then the substitution of these variations may be desirable. Otherwise, if $r \approx a\ \forall t$, and e is small, the expression may be simplified further:

$$\begin{aligned}\begin{pmatrix}\ddot{x}\\ \ddot{y}\\ \ddot{z}\end{pmatrix} = & \begin{bmatrix} 3n^2 & 0 & -n\frac{a}{h}N_{\mathrm{SRP}} \\ 0 & 0 & \dot{\varphi}\frac{a}{h}\frac{\mathrm{d}}{\mathrm{d}\varphi}(N_{\mathrm{SRP}}) \\ -n\frac{a}{h}N_{\mathrm{SRP}} & -\dot{\varphi}\frac{a}{h}\frac{\mathrm{d}}{\mathrm{d}\varphi}(N_{\mathrm{SRP}}) & -n^2\end{bmatrix}\begin{pmatrix}x\\ y\\ z\end{pmatrix} \\ & + \begin{bmatrix} 0 & 2n & 0 \\ -2n & 0 & 2\frac{a}{h}N_{\mathrm{SRP}} \\ 0 & -2\frac{a}{h}N_{\mathrm{SRP}} & 0\end{bmatrix}\begin{pmatrix}\dot{x}\\ \dot{y}\\ \dot{z}\end{pmatrix}\end{aligned} \tag{40}$$

The position and velocity-associated matrices in Eq. (40) are denoted as $[A_p]$ and $[A_v]$, respectively. Reusing the state representation $\boldsymbol{x} = [x, y, z, \dot{x}, \dot{y}, \dot{z}]^\top$, for which one may write $\dot{\boldsymbol{x}} = [A(t)]\boldsymbol{x}$, the time-varying $[A]$ matrix is:

$$[A] = \begin{bmatrix} 0_{3\times3} & I_{3\times3} \\ A_p & A_v \end{bmatrix} \tag{41}$$

with all components of the linear model defined, the linearized relative orbital motion dynamics can now be expressed in their usual form:

$$\dot{\boldsymbol{x}} = [A(t)]\boldsymbol{x} + [B(t)]\boldsymbol{u} \tag{42}$$

The $[A]$ matrix terms are given in Eqs. 40,41. The control-associated $[B]$ matrix is given in Eq. (22), with the lower 3×3 sub-matrix now pre-multiplied by $[\mathcal{HP}]$ to resolve the resultant control accelerations in the LVLH frame components.

3. Application to spacecraft formation control

This section discusses and demonstrates the implementation of the new SRP-perturbed relative orbital motion model for control.

3.1. Linear SRP-based formation and rendezvous control

Control in this paper is performed using the Linear Quadratic Regulator (LQR), which is for the design of a control input $\boldsymbol{u}$ that minimizes the finite-time cost function shown below, under the action of the linearized dynamics $\dot{\boldsymbol{x}} = [A]\boldsymbol{x} + [B]\boldsymbol{u}$ (Sontag, 1998).

$$J = \frac{1}{2}\int_{t_0}^{t_f}\left(\boldsymbol{x}^\top[Q]\boldsymbol{x} + \boldsymbol{u}^\top[R]\boldsymbol{u}\right)\mathrm{d}t + \frac{1}{2}\boldsymbol{x}_f^\top\left[S_f\right]\boldsymbol{x}_f \tag{43}$$

where $[Q]$ and $[R]$ are the state and control-associated weight matrices, and $\left[S_f\right]$ is the matrix associated with the quadratic final state cost. The solution is given below:

$$\boldsymbol{u} = -[K_x]\boldsymbol{x} \tag{44}$$

The time-varying gain matrix $[K_x]$ is given in terms of $[S]$, obtained by solving the Riccati differential equation with final condition $\left[S(t_f)\right] = \left[S_f\right]$:

$$[K_x] = [R]^{-1}[B]^\top[S] \tag{45}$$

$$[\dot{S}] + [S][A] + [A]^\top[S] - [S][B][R]^{-1}[B]^\top[S] + [Q] = [0] \tag{46}$$

3.2. Controllability analysis

Before the SRP-based control is simulated, controllability analysis provides some insight into the problem. For completeness, the time-varying effects of the SRP perturbation are included in the $[A]$ matrix for the relative motion dynamics.

For an LTV system with n states, if the following is satisfied, the system is controllable (Sontag, 1998):

$$\mathrm{rank}([B_0(t), B_1(t), \ldots, B_{n-1}(t)]) = n \tag{47}$$

where $[B_0] = [B]$ and all other elements are given by the following:

$$[B_{i+1}(t)] = [A(t)][B_i(t)] - \frac{\mathrm{d}}{\mathrm{d}t}[B_i(t)] \tag{48}$$

The rank of the controllability matrix, if less than n, determines the dimension of the controllable subspace.

To facilitate this discussion for SRP-based control, the $[B]$ matrix is now resolved into $\mathcal{H}$:

$$[B] = \begin{bmatrix} 0_{3\times 3} \\ [\mathcal{HN}][\mathcal{NP}][B_C] \end{bmatrix} \tag{49}$$

where $[B_C]$ is the constant part of the $[B]$ matrix:

$$\begin{aligned}[B_C] = \; & 4P(R)\tfrac{A}{m}\left(\left(\bar{a}_2 + 2\overline{\rho s}C_{1(1,1)}\right)C_{1(1,1)}[C_1(\boldsymbol{\sigma}_r)]^\top[\tilde{\boldsymbol{e}}_1] - (1-\overline{ps})\left[\hat{\boldsymbol{e}}_1\hat{\boldsymbol{e}}_1^\top\right][\tilde{\boldsymbol{e}}_1]\right. \\ & \left. + \left(\bar{a}_2 + 4\overline{\rho s}C_{1(1,1)}\right)[C_1(\boldsymbol{\sigma}_r)]^\top\left[\hat{\boldsymbol{e}}_1\hat{\boldsymbol{e}}_1^\top\right][C_1(\boldsymbol{\sigma}_r)]^\top[\tilde{\boldsymbol{e}}_1]\right)\end{aligned} \tag{50}$$

If the reference orientation is sun-facing, then $[C_1(\boldsymbol{\sigma}_r)] = [I_{3\times 3}]$ and a much simpler form is obtained for $[B_C]$:

$$[B_C] = 4P(R)\frac{A}{m}(\bar{a}_2 + 2\overline{\rho s})[\tilde{\boldsymbol{e}}_1] \tag{51}$$

For this controllability analysis, it is assumed that the reference orientation is sun-facing. The rotation from $\mathcal{P}$ to $\mathcal{H}$ is time-varying, and thus the $[B]$ matrix will be time-varying as well. Furthermore, the $[A]$ matrix is time-varying. The time-varying terms in the $[A]$ matrix obtained from Eq. (40) can be expected to evolve slowly compared to the time scale of the relative orbital motion dynamics.

Using the SRP-perturbed system $[A]$ matrix, the controllability matrix is obtained in terms of the $[B_i(t)]$ sub-matrices:

$$[B_i(t)] = [B'_i(t)][B_C] = \begin{bmatrix} [B'_{i(u)}(t)] \\ [B'_{i(l)}(t)] \end{bmatrix}[B_C] \tag{52}$$

where $\left[B'_{i(u)}\right]$ and $\left[B'_{i(l)}\right]$ are the upper and lower sub-matrices of $[B'_i(t)]$ and the time-varying portion $[B'_i(t)]$ can be shown to obey the following recursive relationship and initial values:

$$[B'_{i+1}(t)] = \begin{bmatrix} \left[B'_{i(l)}(t)\right] - \frac{\mathrm{d}}{\mathrm{d}t}\left(\left[B'_{i(u)}(t)\right]\right) \\ \left[A_p\right]\left[B'_{i(u)}(t)\right] + \left[A_v\right]\left[B'_{i(l)}(t)\right] - \frac{\mathrm{d}}{\mathrm{d}t}\left(\left[B'_{i(l)}(t)\right]\right) \end{bmatrix} \tag{53}$$

$$\left[B'_{0(u)}(t)\right] = [0_{3\times 3}], \quad \left[B'_{0(l)}(t)\right] = [\mathcal{HP}] \tag{54}$$

Using Eq. (53), and recalling $[B_0(t)] = [B(t)]$, the next two sub-matrices are shown analytically:

$$[B_1(t)] = \begin{bmatrix} [\mathcal{HP}] \\ [A_v][\mathcal{HP}] - [\mathcal{HP}][\tilde{\omega}_{H,P}] \end{bmatrix}[B_C] \tag{55}$$

$$[B_2(t)] = \begin{bmatrix} [A_v][\mathcal{HP}] - 2[\mathcal{HP}][\tilde{\omega}_{H,P}] \\ [A_p][\mathcal{HP}] + [A_v]^2[\mathcal{HP}] - 2[A_v][\mathcal{HP}][\tilde{\omega}_{H,P}] + [\mathcal{HP}][\tilde{\omega}_{H,P}]^2 - [\dot{A}_v][\mathcal{HP}] \end{bmatrix}[B_C] \tag{56}$$

where $[\tilde{\omega}_{H,P}]$ is an angular velocity term associated with the rotating frames:

$$\frac{\mathrm{d}}{\mathrm{d}t}([\mathcal{HP}]) = [\mathcal{HP}]\left[\tilde{\omega}_{H,P}\right] \tag{57}$$

The matrix $[\tilde{\omega}_{H,P}]$ is skew-symmetric, with the components of the angular velocity of frame $\mathcal{P}$ relative to $\mathcal{H}$, expressed in $\mathcal{P}$ components. Note that it is assumed that angular acceleration terms are zero because the effect of rotating frame angular acceleration terms is quite small for near-circular planetary and spacecraft orbits. Thus, $\left[\dot{\tilde{\omega}}_{H,P}\right] \approx [0_{3\times 3}]$.

The symbolic expressions for each sub-matrix were obtained via MATLAB and saved as functions. To enforce

Table 1
Simulation 1 Physical Parameters.

Parameter	Value
$\text{œ}_0 = (a, e, i, \Omega, \theta)$	$200\text{ km}, 0.0, 86.0^\circ, 0.0^\circ, 0.0^\circ$
$\delta\text{œ}_0 = (\delta a, \delta e, \delta i, \delta\Omega, \delta\theta)$	$0.0\text{ km}, 0.00125, 0.05^\circ, 0.0^\circ, 0.0^\circ$
LVLH Initial Conditions	$\Delta\boldsymbol{r} = -250\hat{\boldsymbol{e}}_r\text{m}, \Delta\boldsymbol{r}\prime = 0.01217\hat{\boldsymbol{e}}_t + 0.004253\hat{\boldsymbol{e}}_n$ m/s
Optical constants	$\frac{A}{m} = 0.5\text{ m}^2/\text{kg}, \overline{B} = 0.8, \overline{s} = 0.7, \overline{\rho} = 0.3$
Primary Body Orbit Radius	$R = 3.5904 \times 10^8$ km (2.4 AU)
Primary Body Orbit Angles	$\kappa = 4^\circ, \varphi_0 = 90^\circ$
Primary Body Physical Parameters	$d = 40\text{ km}, \rho_a = 2.119\text{ g/cm}^3, M = 7.1 \times 10^{16}$ kg

the zero angular acceleration condition, the time-varying angular terms were truncated to their linear approximations, $\theta \approx \theta_0 + nt$ and $\varphi \approx \varphi_0 + \dot{\varphi}t$. The final expression for the controllability matrix is far too long and complex to be included here.

Table 1 gives hypothetical parameters for evaluating the controllability matrix, and for the first set of simulation results to follow this controllability analysis. Note that d is the primary body diameter, ρ_a is the body density, and M is the body mass. Recall that $\overline{s}$ and $\overline{\rho}$ are the specular and diffuse reflectivity coefficients, and $\overline{B}$ is the Lambertian scattering coefficient. The optical parameters for this first result are values corresponding to a completely reflective surface (McInnes, 1999), but adding absorption doesn't affect the conclusion of the controllability analysis. This hypothetical simulation data is representative of some high-altitude orbit over a large asteroid. Only two-body gravity and SRP perturbations are implemented in the truth model, since this paper is primarily concerned with the solar radiation pressure perturbation, which would be a dominant disturbance at this altitude.

Using the parameters in Table 1, the rank of the controllability matrix may be obtained for various times in the simulation. Numerical results show that the rank of the controllability matrix is consistently 6, using the MATLAB `rank` function with the default tolerance. This function uses a singular value decomposition and computes the number of singular values lower than the tolerance. For the `rank` function, the default tolerance given a matrix `B` is computed in MATLAB as `max(size(B))*eps(norm(B))`. Lowering the tolerance (e.g. to 10^{-10}), the rank of the controllability matrix reduces to 4. These numerical results suggest that the system is fully controllable, with kinematic coupling enabling weak controllability of the spacecraft motion along $\hat{\boldsymbol{u}}$.

3.3. Testing the SRP-perturbed relative motion model

First, results are presented to demonstrate that the dynamical model obtained in this paper works as expected. Namely, the model given in Eq. (40) was simulated for 6 chief orbit periods with the data given in Table 1, along with a nonlinear truth model. The results are given in Fig. 3. The system matrix of the SRP model is not re-initialized with an update of chief orbital elements during this time frame. There is close agreement between the SRP model and the nonlinear truth model for the 6 orbits simulated, as can be seen from the plot of position error in Fig. 4. This shows that the linearized SRP model is properly accounting for the SRP disturbance acceleration's effects.

3.4. Controlled simulation results

With the efficacy of the linearized dynamical model demonstrated, finite-time LQR control is now implemented to obtain the optimal control signals $\boldsymbol{u}(t) = \boldsymbol{\sigma}_c(t)$. Of partic-

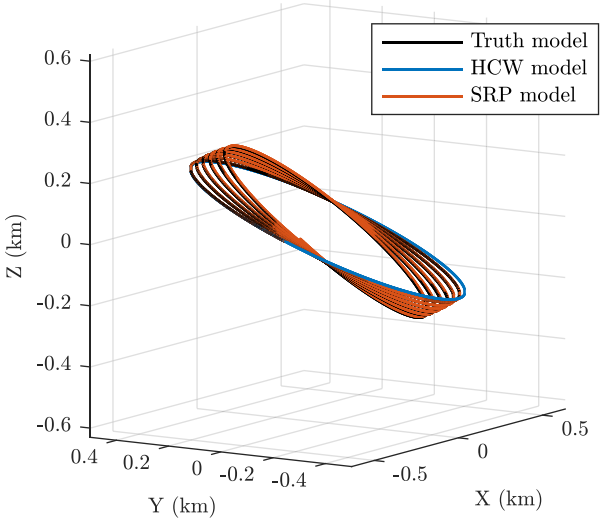

Fig. 3. SRP-Perturbed Relative Motion.

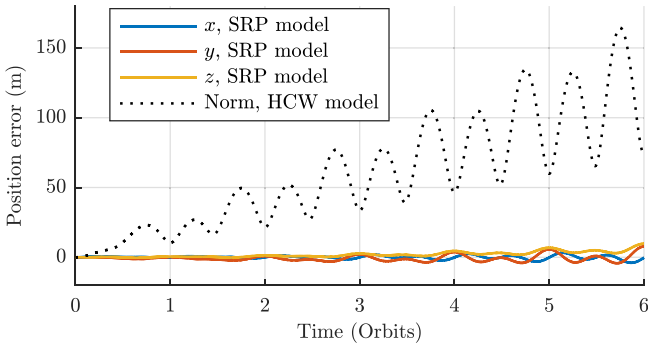

Fig. 4. Model Errors.

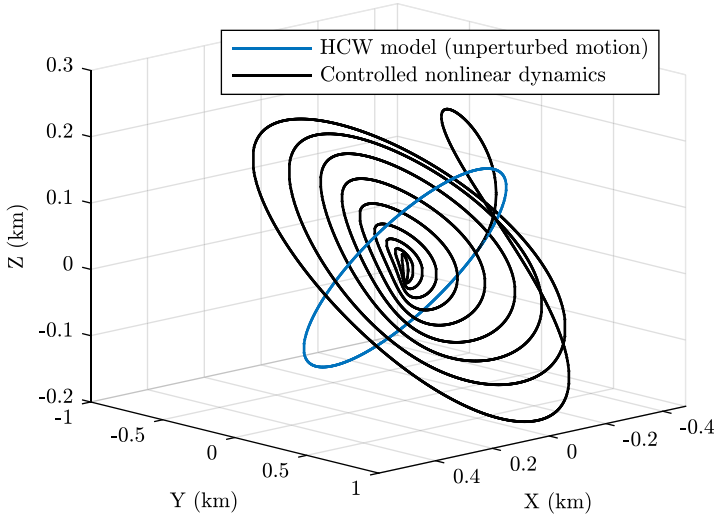

Fig. 5. SRP-Based Control of Relative Motion, Case 1.

ular interest is the full controllability of the system implied by the analysis in the preceding section. It was hypothesized that controllability is weakest in the projection of the motion along $\hat{\boldsymbol{u}}$. Setting the relative motion to take place near the terminator plane allows the motion along $\hat{\boldsymbol{u}}$ to be easily investigated. Without treating the out-of-plane associated elements of the $[Q]$ matrix differently from the in-plane associated elements, simulation results show that the motion in the z direction fails to settle. However, by over-weighing the cost of z and $\dot{z}$ in the dynamics, the controller takes a strategy that seeks to minimize the motion in this mode, by delaying the settling of the x and y motion. The controlled relative motion is given in Fig. 5, showing the deputy relative motion settling to the vicinity of the chief.

The first simulation demonstrates relative motion regulation control to a chief in a terminator orbit. The non-optical physical constants and initial conditions are unchanged from the uncontrolled simulation - thus are given in Table 1. The control parameters and the new optical parameters for this simulation are given in Table 2.

The position deviations and control signals are given in Figs. 6 and 7. The results show that for this case, the controller functions as intended – successfully controlling the deputy spacecraft to very near the origin of the LVLH frame, over the course of one month. This is done with $< 10^\circ$ attitude deviations from the sun-pointing direction. This is important in the context of this work, because the attitude variations must remain small in order for the single-plate SRP model to be accurate.

Table 2
Control Parameters and Optical Parameters for Simulation 1.

Parameter	Value
Q	$Q = I_{6\times6}$, except $Q(3,3) = Q(6,6) = 60$
R	$100 I_{3\times3}$
S_f	$I_{6\times6}$
$t_0, \Delta t, t_f$	$t_0 = 0, \Delta t = 10, t_f = 2581510$ (29.88 days)
Optical constants	$\frac{A}{m} = 0.5\ \mathrm{m}^2/\mathrm{kg}, \overline{B} = 0.6, \overline{s} = 0.25, \overline{\rho} = 0.3$

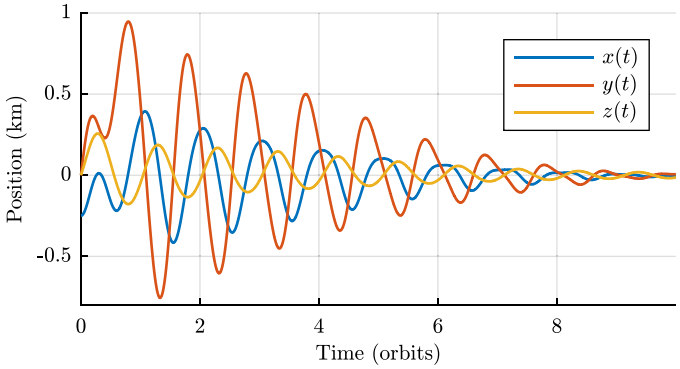

Fig. 6. Controlled Position, Case 1.

The second simulation demonstrates control to change a GEO orbit longitude by 0.544°, or 20 km in the along-track direction, over the course of 30 days. The optical parameters are the same as in the first simulation, but the other physical parameters and the new control parameters are different. These are given in Tables 3 and 4 respectively. This simulation neglects the perturbative effects of lunar and solar gravity, which manifest via a long term (53 year) precession and nutation of the orbit (Anderson et al., 2015). In this particular case, a scale analysis of the lunar gravity perturbation will show that there would be sufficient control authority to cancel such perturbations in addition to controlling the spacecraft to the desired location.

The motion in LVLH x and y components is given in Fig. 8. The z motion is quite insignificant in this case, so it is not shown. Note that the scale of the x motion is magnified in the figure to show the bowed nature of the trajectory followed, and to clearly show the oscillations in the radial direction. Also note the overshoot in the y direction followed by the slow settling behavior around the origin. In

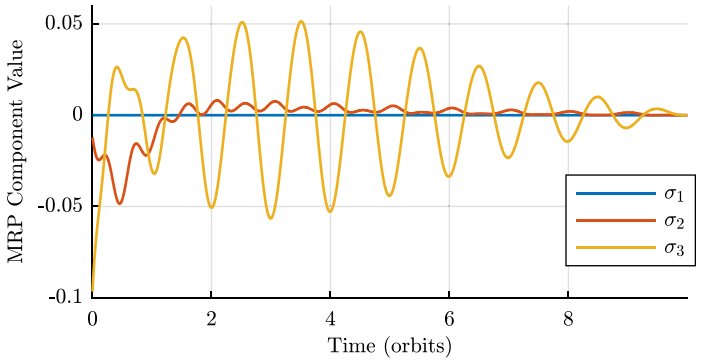

Fig. 7. Control Signals, Case 1.

Table 3
Simulation 2 Physical Parameters.

Parameter	Value
$\text{oe}_0 = (a, e, i, \Omega, \theta)$	42157 km, 0.0, 0.0°, 0.0°, 0.0°
$\delta\text{oe}_0 = (\delta a, \delta e, \delta i, \delta\Omega, \delta\theta)$	0.0 km, 0.0, 0.0°, 0.0°, 0.544°
Primary Body Orbit Radius	$R = 1.496 \times 10^8$ km (1.0 AU)
Primary Body Orbit Angles	$\kappa = 23.5°, \varphi_0 = 90°$
Primary Body Physical Parameters	$r = 6371$ km, $\mu = 398600$ km^3/s^2

Table 4
Control Parameters and Optical Parameters for Simulation 2.

Parameter	Value
Q	$0.5I_{6\times6}$
R	$10^5 I_{3\times3}$
S_f	$S_f = 10^8 I_{6\times6}$, except $S_f(1,1) = 10^{10}$ & $S_f(4,4) = 10^{11}$
$t_0, \Delta t, t_f$	$t_0 = 0, \Delta t = 80, t_f = 2584240$ (30 days)
Optical constants	$\frac{A}{m} = 0.5$ m^2/kg, $\overline{B} = 0.6, \overline{s} = 0.25, \overline{\rho} = 0.3$

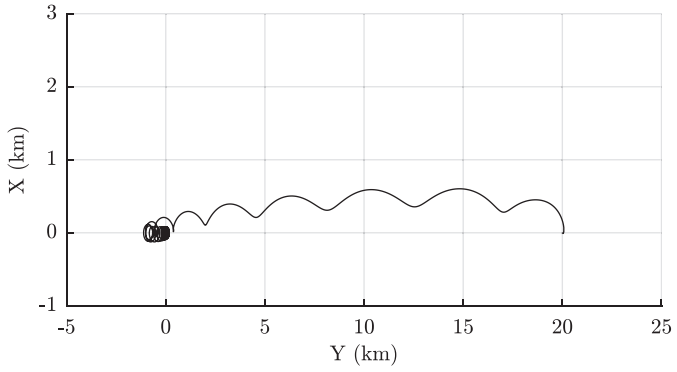

Fig. 8. SRP-Based Control of Relative Motion, Case 2.

practice, the overshoot in y might be undesirable for rendezvous due to the risk of collision, but this problem can be amended with a better choice of control gains and final time. There are two time scales of the settling behavior. Much of the separation is settled in the along-track direction within 15 orbits, but the control action in the remaining orbits slowly dampens out the oscillations

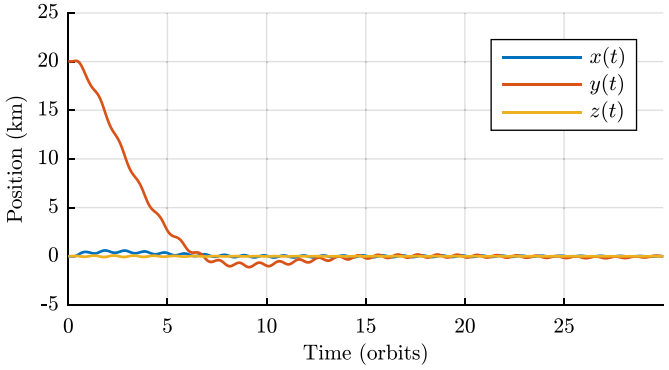

Fig. 9. Controlled Position, Case 2.

mainly in the x and y components. The large final cost on the relative state ensures that in the final 3–4 orbits, the relative motion is further settled (see Fig. 9 and 10).

These results suggest that relatively large maneuvers in the GEO belt are possible with SRP-based linear control, assuming sufficient time is available for such maneuvers. Faster settling results would likely be possible through iteration on the current selection of control parameters, but these results are an adequate demonstration of capability. The results from cases 1 and 2 show that both closed-loop rendezvous control and larger changes to a GEO orbit using a virtual chief are possible using small sustained attitude variations to change the resultant SRP disturbance force. This is simulated for spacecraft with relatively realistic area-to-mass ratios and unremarkable (neither highly reflective or absorptive) optical properties. Simulations with smaller area-to-mass ratios still display the same characteristic behavior, but with longer time spans needed to achieve the same control objectives.

3.5. Practical considerations

For implementing the control strategy introduced in this work, several challenges should be explicitly mentioned and discussed. The first challenge to implementing SRP-based formation control is the general challenge of reliable relative state estimation for spacecraft in a formation. The position of one spacecraft with respect to the other should

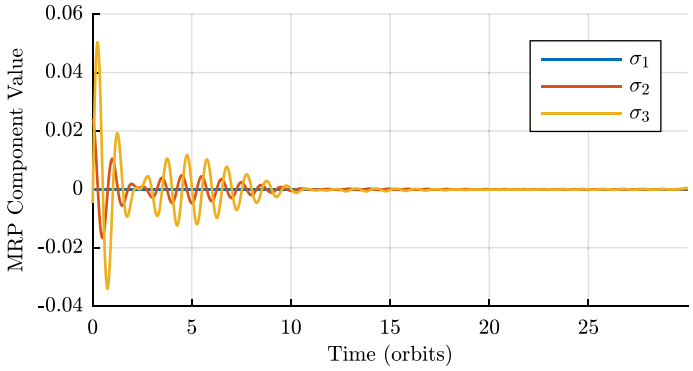

Fig. 10. Control Signals, Case 2.

be known to sufficiently high precision that maneuvers for rendezvous or reconfiguration pose no practical risk of collision. In practice, this might necessitate that the relative state estimation be performed with sensors on board the spacecraft and not rely on differential state measurements from the ground.

A second and equally fundamental challenge is that successful SRP-based formation control is predicated on a sufficiently accurate model of the solar radiation pressure acting on the spacecraft in a formation. However, if the spacecraft in the formation have identical design and are using the same SRP model, then systematic errors in the SRP modeling will partially cancel. In addition, if two spacecraft have the same construction and are subjected to the same orbital environment, then the difference in resultant solar radiation pressure for the same orientation should be quite small. The final challenge for implementation is enforcing that deviations from the reference attitudes remain sufficiently small that the control linearization is not violated. The constraint was enforced in this work via choosing an LQR control weight $[R]$ sufficiently large, but other strategies could be used.

4. Conclusions

This paper derives a new relative motion model accounting for the effects of the solar radiation pressure (SRP) disturbance acceleration on spacecraft relative motion. The kinematics of the SRP-perturbed chief orbit are absorbed into the linearized plant matrix to accommodate infrequent updates of the chief orbit parameters. The model demonstrates the feasibility of SRP-based control in multiple environments of interest for spacecraft with unremarkable geometry and surface optical properties. The model is derived from an existing multi-facet model of SRP force, obtaining an illuminated body averaged single-plate model that should be valid for small angular attitude deviations, especially for spacecraft with large solar arrays, or otherwise relatively flat spacecraft. Numerical simulations of SRP-based control for spacecraft with unremarkable geometric and optical properties establish the feasibility of the use of attitude-dependent SRP force for formation and rendezvous control.

Future work will explore refinements to the methods used in this work, and will detail the limitations of the model and control strategy used in this work. Future work will also include higher-fidelity multi-facet spacecraft SRP modeling that is valid for larger attitude variations, and explorations of how to account for independent articulation of solar arrays in a box-wing spacecraft model. Finally, the study of uncontrolled SRP-perturbed formation dynamics may also continue, with updated models to ease the restrictions made by assumptions in deriving this model.

A multi-fidelity modeling approach could enable a low-level control strategy (linear or otherwise) to be corrected for high precision SRP-based control. Look-up tables generated in advance (or series fits of such data) could take place of the linearized approximation of the attitude-dependent variations in the magnitude and direction of the resultant SRP acceleration. This work is thus the first step towards a goal of accurate high-fidelity SRP-based formation and orbit control.

Acknowledgements

This work was supported by the U.S. Department of Defense through the National Defense Science and Engineering Graduate Fellowship (NDSEG) Program.

References

Anderson, P., McKnight, D.S., Pentino, F.D., Schaub, H., 2015. Operational considerations of GEO debris synchronization dynamics. In: 66th International Astronautical Conference, October 12–16, 2015. Jerusalem, Israel. International Astronautical Federation.

Burnett, E.R., Butcher, E.A., 2018. Linearized relative orbital motion dynamics in a rotating second degree and order gravity field. In: AAS/AIAA Astrodynamics Specialist Conference, August 19–23, 2018. Snowbird, Utah, USA. Advances in the Astronautical Sciences, vol. 167. American Astronautical Society, pp. 3463–3482.

Byram, S.M., Scheeres, D.J., 2009. Stability of sun-synchronous orbits in the vicinity of a comet. J. Guid. Control Dyn. 32 (5), 1550–1559.

Casotto, S., 2016. The equations of relative motion in the orbital reference frame. Celestial Mech. Dyn. Astron. 124 (3), 215–234.

Clohessy, W.H., Wiltshire, R.S., 1960. Terminal guidance system for satellite rendezvous. J. Aerospace Sci. 27 (9), 653–658.

Dachwald, B., 2010. Solar sail dynamics and control. In: Encyclopedia of Aerospace Engineering. John Wiley & Sons.

Danielson, D.A., 2003. Vectors and Tensors in Engineering and Physics. Westview Press.

Dankowicz, H., 1994. Some special orbits in the two-body problem with radiation pressure. Celestial Mech. Dyn. Astron. 58 (4), 353–370.

Farrés, A., Folta, D., Webster, C., 2017. Using spherical harmonics to model solar radiation pressure accelerations. In: AAS/AIAA Astrodynamics Specialist Conference, August 20—24, Stevenson, WA, USA. American Astronautical Society.

Foster, C., Mason, J., Vittaldev, V., Leung, L., Beukelaers, V., Stepan, L., Zimmerman, R., 2018. Constellation phasing with differential drag on planet labs satellites. J. Spacecraft Rockets 55 (2), 473–483.

Howell, S.B., Sobeck, C., Haas, M., Still, M., Barclay, T., 2014. The K2 Mission: Characterization and Early Results. Publications of the Astronomical Society of the Pacific.

Kikuchi, S., Howell, K.C., Tsuda, Y., Kawaguchi, J., 2017. Orbit-attitude coupled motion around small bodies: Sun-synchronous orbits with sun-tracking attitude motion. Acta Astronaut. 140, 34–48.

Lantukh, D., Russell, R.P., Broschart, S.B., 2015. Heliotropic orbits at oblate asteroids: balancing solar pressure and J2 perturbations. Celestial Mech. Dyn. Astron. 121 (171–190).

McInnes, C.R., 1999. Solar Sailing: Technology, Dynamics, and Mission Applications. Springer-Verlag.

Misra, G., Izadi, M., Sanyal, A., Scheeres, D.J., 2016. Coupled orbit-attitude dynamics and relative state estimation of spacecraft near small solar system bodies. Adv. Space Res. 57 (8), 1747–1761.

Oguri, K., McMahon, J.W., 2018. SRP-based orbit control with application to small body landing. In: AAS/AIAA Astrodynamics Specialist Conference, August 19–23, 2018. Snowbird, Utah, USA. Advances in the Astronautical Sciences, vol. 167. American Astronautical Society.

O'Shaughnessy, D.J., McAdams, J.V., Williams, K.E., Page, B.R., 2009. Fire sail: messenger's use of solar radiation pressure for accurate mercury flybys. In: AAS Spaceflight Mechanics Meeting, February 8–12, 2009. Savannah, GA, USA. American Astronautical Society.

Parsay, K., Schaub, H., 2015. Designing solar sail formations in sun-synchronous orbits for geomagnetic tail exploration. Acta Astronaut. 107, 218–233.

Parsay, K., Schaub, H., 2016. Drift-free solar sail formations in elliptical sun-synchronous orbits. Acta Astronaut. 139, 201–212.

Prussing, J.E., Conway, B.A., 2013. Orbital Mechanics. Oxford University Press.

Schaub, H., Junkins, J.L., 2018. Analytical Mechanics of Space Systems, fourth ed. AIAA Education Series, Reston, VA.

Scheeres, D.J., 2007. The dynamical evolution of uniformly rotating asteroids subject to YORP. Icarus 188, 430–450.

Scheeres, D.J., 2012. Orbital Motion in Strongly Perturbed Environments. Springer-Verlag, Berlin Heidelberg.

Sontag, E., 1998. Mathematical Control Theory: Deterministic Finite Dimensional Systems. Springer.

Vallado, D.A., 2007. Fundamentals of Astrodynamics and Applications, third ed. Microcosm Press.